Markov state model of the two-state behaviour of water

Hamm, Peter

Abstract: With the help of a Markov State Model (MSM), two-state behaviour is resolved for two computer models of water in a temperature range from 255 K to room temperature (295 K). The method is first validated for ST2 water, for which the so far strongest evidence for a liquid-liquid phase transition exists. In that case, the results from the MSM can be cross-checked against the radial distribution function g(5)(r) of the 5th-closest water molecule around a given reference water molecule. The latter is a commonly used local order parameter, which exhibits a bimodal distribution just above the liquid-liquid critical point that represents the low-density form of the liquid (LDL) and the high density liquid. The correlation times and correlation lengths of the corresponding spatial domains are calculated and it is shown that they are connected via a simple diffusion model. Once the approach is established, TIP4P/2005 will be considered, which is the much more realistic representation of real water. The MSM can resolve two-state behavior also in that case, albeit with significantly smaller correlation times and lengths. The population of LDL-like water increases with decreasing temperature, thereby explaining the density maximum at 4 degrees C along the lines of the two-state model of water. Published by AIP Publishing.

DOI: https://doi.org/10.1063/1.4963305

Markov state model of the two-state behaviour of water

Peter Hamm

Citation: J. Chem. Phys. **145**, 134501 (2016); doi: 10.1063/1.4963305
View online: http://dx.doi.org/10.1063/1.4963305
View Table of Contents: http://aip.scitation.org/toc/jcp/145/13
Published by the American Institute of Physics

Markov state model of the two-state behaviour of water

Peter Hamm
Department of Chemistry, University of Zurich, Zurich, Switzerland

(Received 9 August 2016; accepted 8 September 2016; published online 3 October 2016)

With the help of a Markov State Model (MSM), two-state behaviour is resolved for two computer models of water in a temperature range from 255 K to room temperature (295 K). The method is first validated for ST2 water, for which the so far strongest evidence for a liquid-liquid phase transition exists. In that case, the results from the MSM can be cross-checked against the radial distribution function $g_5(r)$ of the 5th-closest water molecule around a given reference water molecule. The latter is a commonly used local order parameter, which exhibits a bimodal distribution just above the liquid-liquid critical point that represents the low-density form of the liquid (LDL) and the high density liquid. The correlation times and correlation lengths of the corresponding spatial domains are calculated and it is shown that they are connected via a simple diffusion model. Once the approach is established, TIP4P/2005 will be considered, which is the much more realistic representation of real water. The MSM can resolve two-state behavior also in that case, albeit with significantly smaller correlation times and lengths. The population of LDL-like water increases with decreasing temperature, thereby explaining the density maximum at 4 °C along the lines of the two-state model of water. *Published by AIP Publishing.* [http://dx.doi.org/10.1063/1.4963305]

I. INTRODUCTION

The so-called two-state model of water has been put forward more than a century ago[1] in an attempt to explain the anomalous thermodynamic properties of water, most notably the density maximum at 4 °C, by a shifting equilibrium between a low-density form of the liquid (LDL) and a high density liquid (HDL). That is, while a "simple liquid" would monotonically increase in density when decreasing temperature due to the anharmonic interaction potentials, a decreasing amount of HDL counteracts that trend and eventually leads to a decreasing density with decreasing temperature.[2] The two-state model of water has seen a revival more recently by the liquid-to-liquid phase transition hypothesis of Stanley and coworkers,[3,4] according to which a second critical point exists for water in the deeply super-cooled regime that separates LDL and HDL in a discontinuous phase transition. In part, the liquid-to-liquid phase transition hypothesis is motivated by the corresponding forms of amorphous ice, i.e., low-density amorphous (LDA) ice *versus* high-density amorphous (HDA) ice. In either case, the two forms are characterized as either a predominantly hydrogen-bonded tetrahedral structure (LDL and LDA), or as interpenetrating hydrogen bond networks that lead to waters in interstitial sites (HDL and HDA).

While the existence of the two forms of amorphous ice is well established, the discussion of liquid-to-liquid phase transition hypothesis remains very controversial. The second critical point is supposed to lie in the so-called "no-mans land," which is difficult to reach experimentally, since water homogeneously nucleates very quickly within about 1 ms in that regime.[5] Only very recently, experiments attempted to reach into "no-mans land" from either the top[5] or the bottom.[6] Even for computer models of water, no agreement has been reached. Conflicting results have been discussed as either two metastable phases[7–10] or as an artifact from non-equilibrated molecular dynamics (MD) simulations.[11–14] Some authors argue that relatively minor changes in the force field, i.e., the treatment of the long range electrostatics, can make the difference of whether or not a liquid-to-liquid phase transition exists for a particular water model (Refs. 8 and 9 *versus* Refs. 11 and 12), whereas others claim that it is a universal property of any tetrahedrally shaped force field in a sizeable parameter range.[15,16] According to Chandler[14] as well as Binder,[17] diverging correlation lengths coincide with diverging relaxation times when approaching a critical point, hence the equilibration time would inevitably exceed that of spontaneous nucleation. However, it has also been argued[10,17] that this time scale issue does not necessarily preclude a liquid-to-liquid phase separation.

It is a central claim of the liquid-to-liquid phase transition hypothesis that its reminiscence is still observable at ambient temperatures along the Widom line. The transition between both forms then is no longer discontinuous, rather both forms are believed to coexist in spatial domains, whose correlation length decreases as the temperature increases. That scenario is the two-state model of water. However, even if the liquid-to-liquid phase transition does exist, it is not clear whether two-state behavior survives into ambient conditions. This question has been addressed from an experimental point of view, but remained controversial as well. That is, the enhanced scattering amplitude for very small angles in X-ray scattering experiments of room temperature water has been interpreted in terms of these spatial domains,[18] while others have interpreted essentially the same experimental observation as continuous—in contrast to bimodal—density fluctuations, as they are expected from the isothermal compressibility.[19]

Identifying two-state behaviour above the liquid-to-liquid phase transition point requires a local order parameter that discriminates whether a given water molecule belongs to a LDL or to a HDL domain. Two order parameters have been used in this regard: The radial distribution function $g_5(r)$ of the 5th-closest water molecule around a given reference water molecule,[20] as well as the so-called local structure index (LSI),[21,22] which considers all waters in the first and the second coordination layers and evaluates their distances to the central water (for details see Eq. (1) of Ref. 21). Both order parameters reveal a bimodal distribution to some extent, however, in the case of $g_5(r)$ only for temperatures just above the hypothesized liquid-liquid phase transition point.[20] The peak at the larger distance in $g_5(r)$ corresponds to a 5th water that is in the second coordination layer of a tetrahedral structure (i.e., a water in a LDL domain), while the peak at smaller distances corresponds to an interstitial water (i.e., a water in an HDL domain). The LSI distribution, on the other hand, remains bimodal even at ambient temperatures, but only if it is calculated after energy-minimizing a snapshot structure taken from a MD simulation.[21,22] This procedure quenches the liquid into the amorphous ices LDA and HDA at 0 K. The existence of these amorphous forms of ice is not questioned, however, it is not clear to what extent the quenching procedure preserves the structure of the liquid. Other order parameters, in particular the local density derived from the volume of the Voronoi polyhedron (i.e., all points that are closer to the oxygen atom of the reference water than to any other oxygen atom), do not reveal any bimodal distribution.[22,23] However, a geometry-based, predetermined order parameter will essentially always underestimate barrier heights between free-energy basins, up to the point that it completely misses a barrier, as it typically fails to incorporate all relevant degrees of freedom.[24]

Here, a kinetic approach is taken to detect and to analyze two-state behaviour of water above the liquid-to-liquid phase transition. The approach does not have to start from a predetermined order parameter. Rather, it first groups snap-shot structures taken from a MD simulation into structurally highly resolved microstates, using the RMSD as a measure of similarity. Subsequently, a transition probability matrix is constructed between these microstates, which is analyzed as a Markov State Model (MSM). To that end, the eigenvalues of the transition probability matrix are calculated, which are related to the time-constants of various relaxation processes.[25,26] MSMs lead to a physically interpretable coarse-graining of the system under study, if one finds a separation of time scales between one, or very few, significant time-constants, which are slow compared to all other time-constants. In that case, the slow time-constants are interpreted as transition times between a small number of free-energy basins, whereas the fast time-constants represent the kinetics within the basins.

MSMs are commonly applied to proteins,[25–28] and will be adapted here to study water. The approach is first established for ST2-water.[29] That computer model of water is not chosen because it is believed to be a particularly good representation of real water, but because the so far strongest evidence for a liquid-to-liquid phase transitions (albeit not generally accepted[11–14]) has been provided for that model,[7,8,20,30–33] most notably in the recent work by Debenedetti and co-workers.[9] If ST2 water indeed exhibits a liquid-to-liquid phase transition, it must show two-state behaviour at least at temperatures just above the liquid-to-liquid phase transition point. From all models of water, for which a liquid-to-liquid phase transition has been hypothesized, ST2 water reveals the highest temperature for the liquid-to-liquid phase transition point with estimates ranging from 237 K[31] to 247 K,[30] depending on the way how the long-range electrostatics is treated (Ewald *versus* reaction field, respectively). The high temperature of the liquid-to-liquid phase transition point renders the dynamics comparatively fast, allowing one to converge simulations relatively easily. The melting point of ST2 water at ambient pressure has been estimated to lie around 300 K.[34] It will be shown that two-state behaviour can indeed be identified as local free energy minima of the MSM that correlates well with the radial distribution function $g_5(r)$ of the 5th-closest water molecule. Temporal and spatial correlation functions will then be discussed in dependence of temperature.

Once the method is validated for ST2 water, we will turn to TIP4P/2005 water,[35] which in terms of its thermodynamic properties is believed to be the best possible among all rigid non-polarizable water models.[36] In particular, it has been fitted to reproduce density maximum at 4 °C,[35] while its melting point is at 252 K. If a central claim of the two-state hypothesis is correct and the density maximum is indeed related to a shift in equilibrium between LDL and HDL, one should expect to resolve these states in a MSM even at ambient temperatures. Also for TIP4P/2005 water, evidence for a liquid-to-liquid phase transition has been provided,[37–40] albeit much less thoroughly than for ST2 water. Furthermore, the criticism that the observation of a liquid-to-liquid phase transition is an artifact of non-equilibrated MD simulation[11–14] is probably even more relevant in the case of TIP4P/2005 water, since the hypothesized phase transition point is much lower in temperature, i.e., at ≈180-190 K.[37–40] It will be shown that the MSM can resolve two-state behaviour also for TIP4P/2005 water in a temperature range that covers the density maximum, with a shift in equilibrium between HDL and LDL domains that is exactly as expected for the two-state model of water.

II. METHODS

A. MD simulation

For ST2 water, the same parametrization as in Refs. 30, 32, and 33 has been used, i.e., the charge geometry of Ref. 29 augmented with a screening function for the Coulomb interaction for small distances and a switching function for long distances with cut-off 7.8 Å, the Lennard Jones interactions cut-off at the same distance, and the long-range electrostatics approximated by the reaction field.[41] The water molecules were kept rigid by Shake.[42] Using a home-written code, a box with 5000 water molecules has been simulated with time step 2 fs in the *NVT* ensemble with box-sizes varied from 54.58 Å to 53.44 Å, corresponding to densities varied from 0.92 g/cm^3 to 0.98 g/cm^3, respectively, and thermostated with a coupling time-constant of 1 ps. The MD setup has been

checked against the results of Ref. 32, in particular with regard to the diffusion constant and the inflection point obtained in the (p,V)-diagram when approaching the liquid-to-liquid phase transition point. For each state point in the phase diagram considered, the simulation box has been pre-equilibrated for at least 10 ns, revealing the mean square displacement of the water molecules of ≈28 Å (i.e., 10 inter-water distances) for the slowest case considered here (ST2 water at T = 255 K and density 0.92 g/cm^3). A similar criterion has been used before as validation of equilibration.[32] The production runs were 1 ns long with saving time 20 fs.

TIP4P/2005[35] was simulated in Gromacs[43] with the long range electrostatic forces approximated by the particle-mesh-Ewald approximation and the Lennard-Jones interactions truncated at 10 Å. The goal was to observe two-state behavior across the density maximum of water at an ambient pressure of 1 bar. To that end, simulation boxes have been pre-equilibrated for 10 ns in the NpT ensemble at 1 bar in a temperature range from 255 K to 295 K in 5 K steps, and the resulting averaged box-sizes have been determined. That box-size as a function of temperature has then been fitted to a cubic function, and the simulation box has been equilibrated a second time in the NVT ensemble for 10 ns using box-sizes from that fit. The subsequent production runs were 1 ns in the NVT ensemble. All other simulation parameters were the same as for ST2 water.

B. RMSD calculation

As a first step to define a MSM, one needs a measure of similarity of the local structures around two water molecules. Motivated by the observation that the 5th-closest water molecule around a central reference water is to a certain extent decisive to distinguish HDL and LDL, i.e., by the fact that $g_5(r)$ exhibits a bimodal distribution at least close to the liquid-liquid phase transition point,[20] water clusters were cut out from the full simulation box, which included a central reference water together with the five closest waters around it. These $(H_2O)_6$ clusters would typically contain the four water molecules that are hydrogen-bonded to the central reference water in a tetrahedral structure as well as the 5th-closest water, from which $g_5(r)$ is calculated.

As a measure of similarity of two such $(H_2O)_6$ clusters i and j, the RMSD was calculated as

$$\mathrm{rmsd}(i,j)^2 = \min_{\mathbf{d},\mathbf{Q},\mathbf{P}} \frac{1}{N}\sum_{k=1}^{N} \left|\mathbf{x}_k^{(i)} - \mathbf{d} - \mathbf{Q}P_{kl}\mathbf{x}_l^{(j)}\right|^2, \qquad (1)$$

where the sum runs over the $N = 6$ oxygen atoms in the water clusters. Here, $\mathbf{x}_k^{(i)}$ are the Cartesian coordinates of the kth atom in water cluster i. Following well established procedures,[44–46] both water clusters were optimally superimposed by first overlying their center of masses via a translation $\mathbf{d}$, and by a subsequent unitary transformation $\mathbf{Q}$ finding the global minimum for all $5! = 120$ permutations P_{kl} of the five indistinguishable waters surrounding the central reference water. There is no closed algorithm that finds that global minimum within polynomial time,[46] but since the number of permutations is not very large, all were explored explicitly (however, that issue severely limits the number of molecules in the water cluster that could potentially be considered). The optimal unitary transformation $\mathbf{Q}$ has been determined via a singular value decomposition (SVD),[47] which for this problem is superior compared to the method based on quaternions,[45] as the SVD also includes improper rotations, i.e., a rotation combined with a reflection (the water clusters are not expected to be chiral).

C. Building microstates

As a second step towards a MSM, the *per se* continuous space of $(H_2O)_6$ structures needs to be discretized into highly resolved microstates. These microstates ideally should have roughly the same volume to avoid an erroneous entropy contribution to the free energy of the microstate. To that end, one may define a small cut-off RMSD, and all $(H_2O)_6$ clusters, whose RMSD to a still-to-be-determined reference cluster is smaller than that cut-off, are lumped into the microstate related to that reference cluster. In the simplest (naïve) implementation, the so-called leader algorithm,[48] one searches for each $(H_2O)_6$ cluster along the MD trajectory whether a reference cluster already exists with an RMSD smaller than the cut-off, in which case the cluster is lumped to that reference cluster. Otherwise, the cluster is considered to be a new reference cluster. That algorithm however has two serious problems. First, it scales very unfavorably as $n_s \cdot n_m$, where n_s is the number of considered snapshots and n_m is the number of microstates. Second and more severely, the final outcome of the MSM strongly depends on the random initial choice of reference clusters. For example, if a reference cluster happens to sit right at the top of a free-energy barrier, it might bridge two free energy basins, which is in particular a problem if the barriers are small as they are in the present case.

To overcome both these problems, the hierarchical algorithm presented in Ref. 49 has been used in a slightly modified form. That is, a tree with total six layers was constructed with decreasing RMSD cut-offs. During a first scan of the MD data (the learning phase of the tree), two situations may occur for each snapshot structure of a water cluster as one proceeds from the top to the bottom of the tree: If the snapshot structure did not agree with any of the already existing nodes within the cut-off of the corresponding layer, a new node was generated as a child. Otherwise, the snapshot structure was added to the node with the smallest RMSD, whose centroid structure was shifted so that it becomes the average over all snapshot structures within that node (in contrast to Ref. 49, a centroid structure has also been calculated for the lowest tree level). In the second scan of the MD data, the tree as well as the centroid structures were taken from the first scan and kept fixed. The cut-offs were no longer considered; instead, the child with the smallest RMSD was chosen at each level, and the final node reached at the lowest level was called a microstate. Due to the successive filtering, the mean RMSD within these microstates is significantly smaller than the smallest cut-off.

Each water molecule in the simulation box, together with its surrounding 5 closets waters, was considered to be

an independent sample, hence in total $5000 \cdot (1\ \text{ns}/20\ \text{fs}) = 250\,000\,000$ individual $(H_2O)_6$ clusters were used in the microstate analysis. The cut-offs were chosen such that the typical number of children per parent in the tree is 10-30, which was achieved for the series of cut-offs 1.25, 1.05, 0.91, 0.80, 0.72, and 0.65 Å. With these RMSD cut-offs, the procedure revealed ≈18 000 microstates for ST2 water at T = 255 K and density 0.95 g/cm^3 and an average RMSD within each microstate of 0.27 Å.

The algorithm is much more computer-time efficient than a leader algorithm and roughly scales as $n_s \cdot n_m^{1/l}$, where l is the number of levels in the tree. On a single core of a Xeon E5-2690 processor running at 2.9 GHz, it took ≈7 days to analyze the 250 000 000 $(H_2O)_6$ clusters of a 1 ns trajectory (a parallelized version of the code exists as well), and as such is about 25 times slower than calculating the actual MD trajectory with Gromacs on a single core of the same processor. Furthermore, as a consequence of calculating averaged structures of each node in the first scan of the MD data, the nodes drift towards regions of high data density and render the final tree largely independent of the starting point (but not completely independent, e.g., the noise in Fig. 7(c) shown further below originates from the randomness that remains from the starting point in the tree building).

D. Markov state model

Once the microstates were established, a MSM has been constructed along the lines of Ref. 26. To that end, the transition probability matrix is introduced, which describes the probability of a transition from microstate j to i within a lag time τ_{lag}. It can considered to be a time-propagator

$$\rho_i(t + \tau_{lag}) = \sum_j T_{ij}\rho_j(t), \tag{2}$$

where $\rho_i(t)$ is the population of microstate i at time t. The transition probability matrix was estimated from the number of transitions C_{ij} from microstate j to i observed in the MD trajectory

$$T_{ij} = C_{ij}/C_j \tag{3}$$

with $C_j = \sum_j C_{ij}$. Since the MD simulation is in equilibrium, detailed balance $C_{ij} = C_{ji}$ is expected, which however is not obtained exactly due to statistical shot noise (i.e., with an error on the order of $\sqrt{C_{ij}}$). The count-matrix $\mathbf{C}$ has therefore been symmetrized by setting $C_{ij} \leftarrow (C_{ij} + C_{ji})/2$, which is a reasonable approximation in the "data rich regime,"[25,27] in which the simulation is due to the huge amount of samples (more sophisticated algorithms have been proposed for that purpose[25,26]).

Spectral analysis of a MSM calculates the eigenvalues λ_k and corresponding eigenvectors $\boldsymbol{\rho}^{(k)}$ of the transition probability matrix $\mathbf{T}$. By construct (i.e., due to conservation of total probability), the largest eigenvalue is $\lambda_1 = 1$ and the corresponding eigenvector $\boldsymbol{\rho}^{(1)}$ is the equilibrium distribution. This is the stationary solution of Eq. (2). The equilibrium probabilities are all positive $\rho_i^{(1)} > 0$ and normalized $\sum_i \rho_i^{(1)} = 1$. Subsequent smaller eigenvalues describe relaxation processes with time-constants

$$\tau_k = -\frac{\tau_{lag}}{\ln(\lambda_k)}. \tag{4}$$

The corresponding eigenvectors $\boldsymbol{\rho}^{(k)}$ contain the change of population during that relaxation process with positive as well as negative components $\rho_i^{(k)}$ and $\sum_i \rho_i^{(k)} = 0$ for all $k \geq 2$.

The transition probability matrix $\mathbf{T}$ is not symmetric. For the numerical solution of the eigenvalue problem, it is advantageous to introduce the symmetric matrix

$$T'_{ij} \equiv \sqrt{T_{ij}T_{ji}} = T_{ij}\sqrt{\frac{T_{ji}}{T_{ij}}} = T_{ij}\sqrt{\frac{C_j}{C_i}} = T_{ij}\sqrt{\frac{\rho_j^{(1)}}{\rho_i^{(1)}}}, \tag{5}$$

where detailed balance has been used in the second step. The eigenvectors of $\mathbf{T}'$, $\boldsymbol{\rho}'^{(k)}$, are orthonormal. From the last equality in Eq. (5), it is easy to see that the eigenvalues of $\mathbf{T}$ are the same as those of $\mathbf{T}'$, and that one obtains for the corresponding eigenvectors

$$\rho_i^{(k)} = \rho_i'^{(k)} \cdot \sqrt{\rho_i^{(1)}} = \rho_i'^{(k)} \cdot \rho_i'^{(1)}. \tag{6}$$

The matrix $\mathbf{T}'$ is quite large but sparse. As one is interested only in a few largest eigenvalues, they can easily be calculated with not too many Lanczos iterations. Occasionally, isolated microstates lead to spurious eigenvalues/eigenvectors, which can easily be filtered out, since their participation ratio

$$\sum_i \left(\rho_i'^{(k)}\right)^4 \tag{7}$$

is close to 1.

In analogy to molecular orbitals,[50] it is instructive to localize the eigenvectors by a unitary transformation $\mathbf{U}$ in a subspace of the s significant eigenvectors

$$\boldsymbol{\rho}'^{(k,loc)} = \sum_{k,l=1}^{s} U_{kl}\boldsymbol{\rho}'^{(l)}. \tag{8}$$

As a criterion of localization, the combined participation ratio

$$\max_{\mathbf{U}} \sum_{k=1}^{s} \sum_i \left(\rho_i'^{(k,loc)}\right)^4 \tag{9}$$

is iteratively maximized with respect to $\mathbf{U}$ using the algorithm described in Ref. 50. The resulting probabilities have arbitrary signs, which were chosen such that $\sum_i \rho_i'^{(k,loc)} > 0$. Finally, the localized probabilities are defined in analogy to Eq. (6),

$$\rho_i^{(k,loc)} = \rho_i'^{(k,loc)} \cdot \rho_i'^{(1)}. \tag{10}$$

Note that the densities defined in this way are not strictly positive (albeit positive values dominate, see Fig. 1(d) below), and furthermore

$$N \equiv \sum_{i,k} \rho_i^{(k,loc)} \neq 1. \tag{11}$$

The localized probabilities therefore were divided by N in order to normalize the total probability.

It has been verified that the results of the MSM (discussed below) are very robust and depend only minimally on the parameters of the analysis, such as the length or saving time of the MD simulation, the cut-offs in the microstate algorithm, or the lag-time in the MSM.

E. Illustration of the Markov state model

Fig. 1 illustrates the various objects just introduced for the simple example of a diffusive process on a one-dimensional double-minimum potential

$$V(x) = 4V_0(x^4 - x^2), \tag{12}$$

where $V_0 = k_BT$ has been chosen (Fig. 1(a)). The problem has been solved by discretizing x-space in the Smoluchowski diffusion equation with a transition probability matrix in the limes $\tau_{lag} \to 0$.[51] The resulting eigenvalue spectrum (Fig. 1(a), inset) contains one slow process with time constant τ_2, which is well separated from all other time constants, and which relates to the exchange kinetics between the two basins of the potential. The corresponding first two eigenvectors $\rho_x^{(1)}$ and $\rho_x^{(2)}$, as well as their localized counterparts $\rho_x^{(loc,1)}$ and $\rho_x^{(loc,2)}$, are shown in Figs. 1(b) and 1(d), respectively. We also see that the ratio

$$p_x \equiv \frac{\rho_x^{(2)}}{\rho_x^{(1)}} \tag{13}$$

shown in Fig. 1(c) is monotonic (in contrast to $\rho_x^{(2)}$) and separates the two basins by switching sign. Hence, it will be used as an order parameter to analyze the MSM.

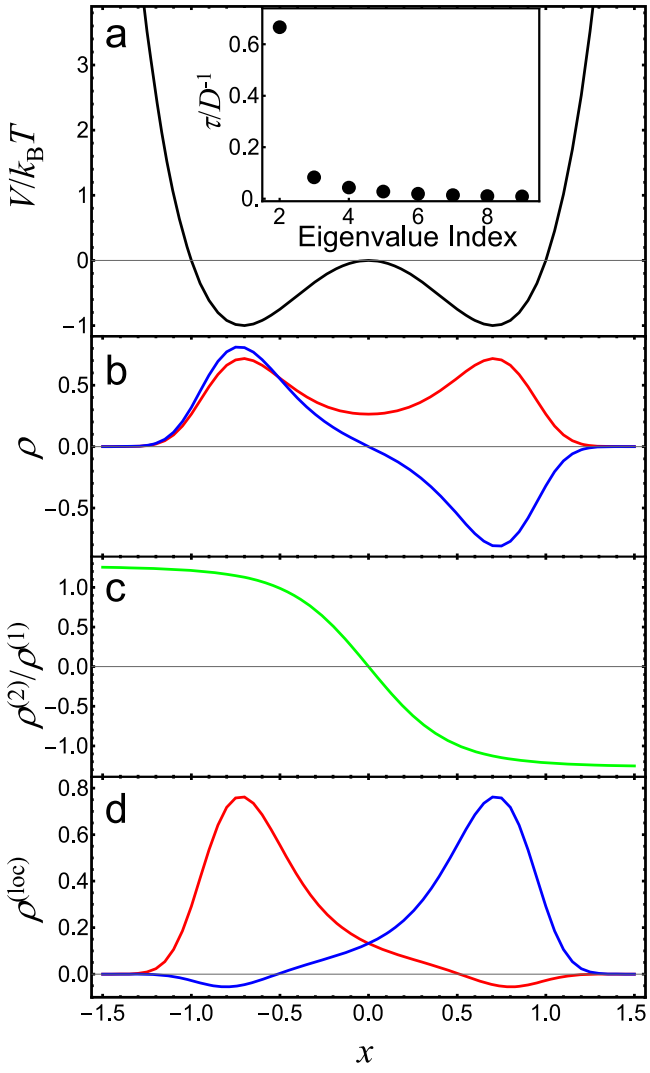

FIG. 1. MSM of a diffusive process on a one-dimensional double-minimum potential (Eq. (12)) with $V_0 = k_BT$. (a) Potential, (b) the eigenvectors $\rho_x^{(1)}$ (red) and $\rho_x^{(2)}$ (blue), (c) the ratio $\rho_x^{(2)}/\rho_x^{(1)}$, and (d) the localized probabilities $\rho_x^{(loc,1)}$ (red) and $\rho_x^{(loc,2)}$ (blue). The inset of panel (a) shows the nine leading time-constants obtained from the spectral analysis of the MSM in units of D^{-1}, where D is the diffusion constant.

III. RESULTS AND DISCUSSION

A. ST2 water

1. Spectral analysis of the MSM

Fig. 2(a) shows the leading time constants of the MSM of ST2 water at constant density 0.95 g/cm^2 and the temperature varied from 255 K (violet) to 295 K (red). A lag-time $\tau_{lag} = 40$ fs has been chosen in the calculation of the transition probability matrix, which revealed the best resolution of the MSM. That is, that lag-time on the one hand maximizes the time scale separation τ_2/τ_3 and at the same time minimizes the number of spurious eigenvalues/eigenvectors resulting from isolated microstates in the transition network. It can be seen in Fig. 2(a) that the slowest time-constant, τ_2, is clearly separated from all others in the full temperature range considered, in analogy to

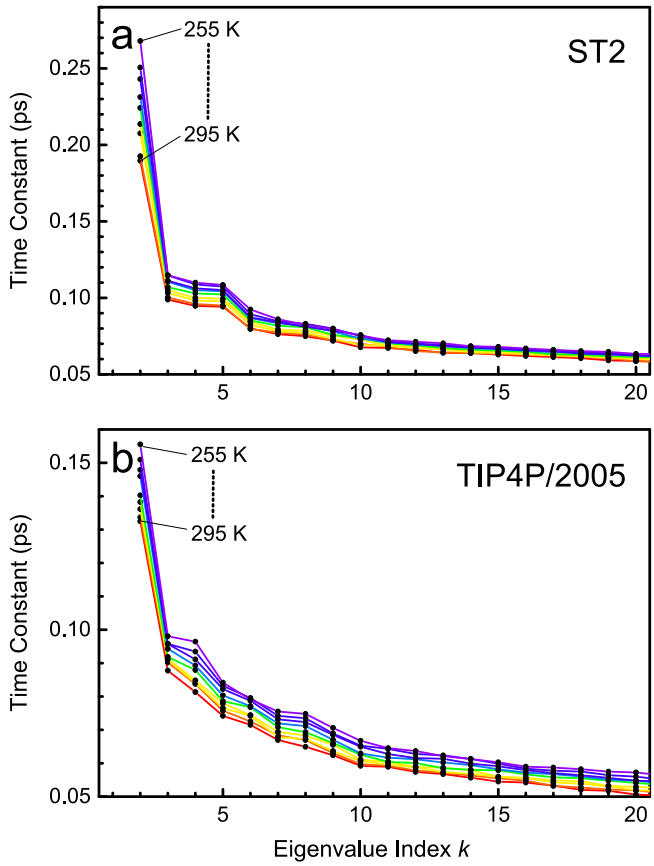

FIG. 2. (a) The leading time constants of the transition probability matrix for ST2 water for the temperature varied from T = 255 K (violet) to 295 K (red) in steps of 5 K at constant density 0.95 g/cm^2. (b) The same for TIP4P/2005 water at constant pressure of 1 bar.

Fig. 1(a) (inset), providing evidence that two-state behaviour is indeed observed. The time scale separation is $\tau_2/\tau_3 \approx 2.3$ at 255 K and decreases with increasing temperature, but a sizeable value of $\tau_2/\tau_3 \approx 1.9$ remains even at room temperature (295 K).

2. Local structure

Figs. 3(a) and 3(b) shows the radial distribution functions $g_5(r)$ of the 5th-closest water molecule around a given reference water molecule for a series of MD simulations of ST2 water, in which either the density is varied at constant temperature 255 K (Fig. 3(a)) or the temperature is varied at constant density 0.95 g/cm^2 (Fig. 3(b)). $g_5(r)$ has been used before as an order parameter that evidences two-state behaviour of water.[20] At a temperature of 255 K, close to the hypothesized liquid-to-liquid phase transition point (247 K), $g_5(r)$ indeed exhibits a bimodal shape with two maxima, whose statistical weights change as the density of the liquid is varied (Fig. 3(a)). That change in weights reflects the shift in the equilibrium between LDL and HDL domains. At higher temperatures ($\gtrsim$270 K), however, the bimodal shape of $g_5(r)$ washes out completely (Fig. 3(b)).

Each water molecule along the MD trajectory is the central reference water of a $(H_2O)_6$ cluster, and as such can be assigned to a microstate i. With that, the distance of the 5th-closest water molecule can be weighted with either $\rho_i^{(1,loc)}$ or $\rho_i^{(2,loc)}$ in the calculation of $g_5(r)$, the result of which is shown in Figs. 3(c) and 3(d). The localized probabilities $\rho_i^{(1,loc)}$ and $\rho_i^{(2,loc)}$ represent the free energy basins that are separated by a time-constant τ_2. Indeed, the radial distribution functions $g_5(r)$ of the two sub-ensembles completely separate the two peaks of the overall $g_5(r)$ shown in Figs. 3(a) and 3(b). This observation proves that the time scale separation found in the MSM (Fig. 2) results in a physically meaningful coarse graining of the network. For example, as the density is increased, the relative fraction of HDL, represented by the $g_5(r)$ peaking at a smaller distance r, increases (Fig. 3(c)). Most importantly, even though the full $g_5(r)$ is no longer bimodal at temperatures $\gtrsim$270 K (Fig. 3(b)), the MSM can still kinetically separate the two sub-populations (Fig. 3(d)). The higher resolution power of the MSM is also evidenced from the distributions of the order parameter p defined in Eq. (13) (Figs. 3(e) and 3(f)), whose bimodal character is more pronounced than that of $g_5(r)$ at all temperatures.

Fig. 4(a) shows the 3D distributions of waters around a central water molecule at temperature 255 K and density 0.95 g/cm^2. The first co-ordination layer shown in grey forms a rather well-defined tetrahedra. The 5th-closest water is shown for the two sub-ensembles corresponding to HDL in blue and LDL in red. In the HDL case, the 5th-closest water populates one of the four interstitial sites between the tetrahedra of the first co-ordination layer. The red lobes of LDL, on the other hand, are arranged in triangulars around the waters of the first co-ordination layer (shown in grey), hence, they are part of the next co-ordination layer in a tetrahedral structure. These red lobes appear to be too

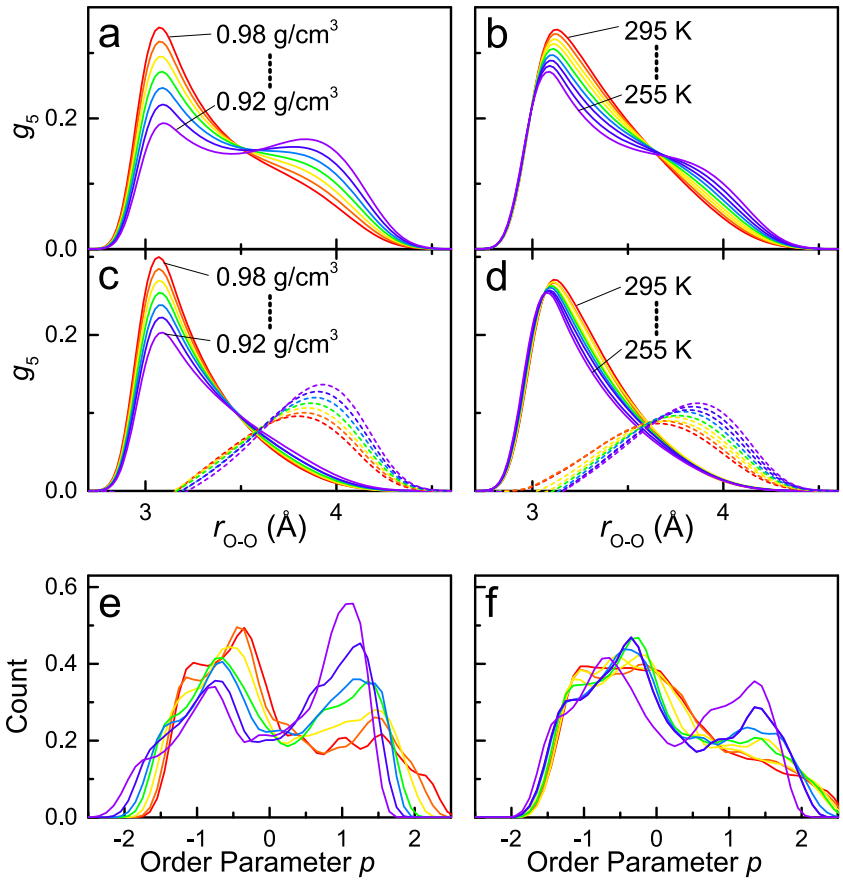

FIG. 3. (a) Radial distribution functions $g_5(r)$ of the 5th-closest water molecule around a central reference water molecule for ST2 water with the density varied from 0.92 g/cm^2 (violet) to 0.98 g/cm^2 (red) in steps of 0.01 g/cm^2 at constant T = 255 K, and in (b) with the temperature varied from T = 255 K (violet) to 295 K (red) in steps of 5 K at constant density 0.95 g/cm^2. Panels (c) and (d) show the same, but weighting each MD snapshot with the 2 localized probabilities $\boldsymbol{\rho}^{(1,loc)}$ and $\boldsymbol{\rho}^{(2,loc)}$ calculated via Eq. (10). Panels (e) and (f) show the corresponding distributions of the order parameter p defined in Eq. (13).

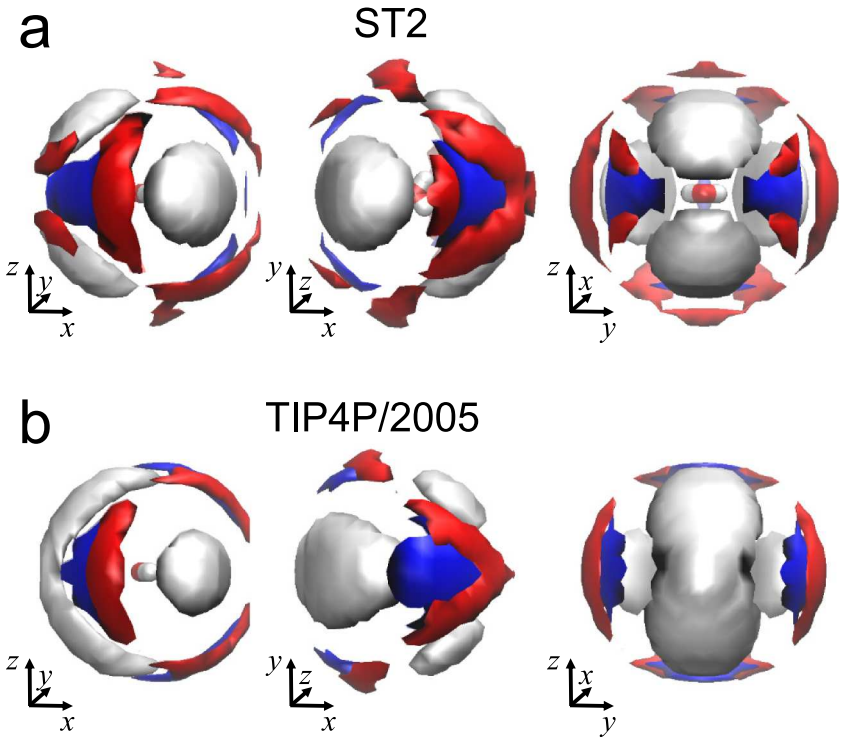

FIG. 4. (a) Oxygen distributions in 3D around a central water molecule for ST2 water at temperature 255 K and density 0.95 g/cm^2. The first coordination layer is shown in grey, the distribution of the 5th closest water molecule weighted with $\rho^{(1,loc)}$ corresponding to the smaller distance (HDL) in blue, and that weighted with $\rho^{(1,loc)}$ corresponding to the larger distance (LDL) in red. (b) Same for TIP4P/2005 water at temperature 255 K and pressure 1 bar.

close to the central water to be consistent with a tetrahedral structure. However, for that one needs to keep in mind that we consider here the 5th-closest water only, and not the in total 12 waters of the second co-ordination layer, hence the presentation of Fig. 4(a) over-emphasizes the low-distance edge of the distribution of waters in the second coordination layer.

3. Time and spatial correlation functions

Fig. 5(a) shows the time-correlation functions of the order parameter p (defined in Eq. (13))

$$c_t(t) \equiv \langle p(0)p(t)\rangle \tag{14}$$

with $p(t) \equiv p_{i(t)}$, and where the average $\langle \ldots \rangle$ goes over time and all water molecules. It follows from the normalisation of the eigenvectors that the mean of the order parameter vanishes, $\langle p \rangle = 0$, hence $c_t(t) \xrightarrow{t\to\infty} 0$, and that the correlation function is normalized, $c_t(0) = 1$. At all temperatures, the correlation function initially decays highly non-exponentially, but eventually turns into an exponential tail, whose time constant strongly depends on temperature. The thin black lines in Fig. 5(a) represent exponential fits of the tong-time tail of $c_t(t)$, whose time-constants τ_c are summarized in Fig. 6(c) (black).

The time scale of the long-time tail is significantly slower than the time-constant τ_2 obtained from the spectral analysis of the MSM (Fig. 2), e.g., 100 ps *versus* 0.27 ps for temperature 255 K and density 0.95 g/cm^2. Rather, τ_2 from the MSM roughly coincides with the time scale of the initial drop of $c_t(t)$ (Fig. 5(a), inset). The highly non-exponential decay of $c_t(t)$ emphasized that the current order parameter does not reveal Markovian dynamics despite the fact that a MSM can resolve the sub-ensembles.

The dynamics is non-Markovian, since the order parameter considers only the local structure around a given water molecule, while longer-lived spatial domains exist,

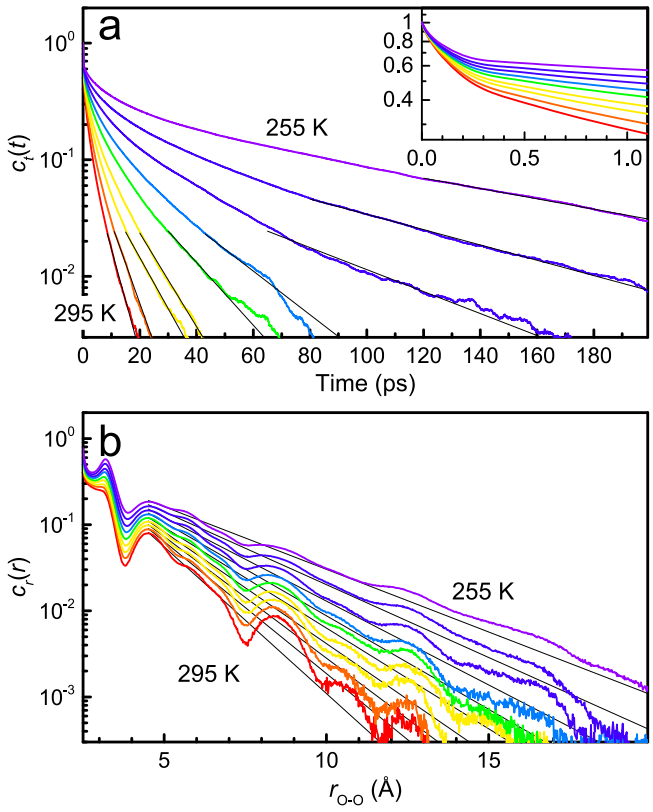

FIG. 5. (a) Time-correlation function $c_t(t)$ and (b) spatial correlation function $c_r(r)$ for ST2 water at density 0.95 g/cm^2 and the temperature varied from T = 255 K (violet) to 295 K (red). The inset of panel a focuses into the initial drop of $c_t(t)$. The thin black lines represent exponential fits to the long-time or large-distance tails of $c_t(t)$ and $c_r(r)$, respectively.

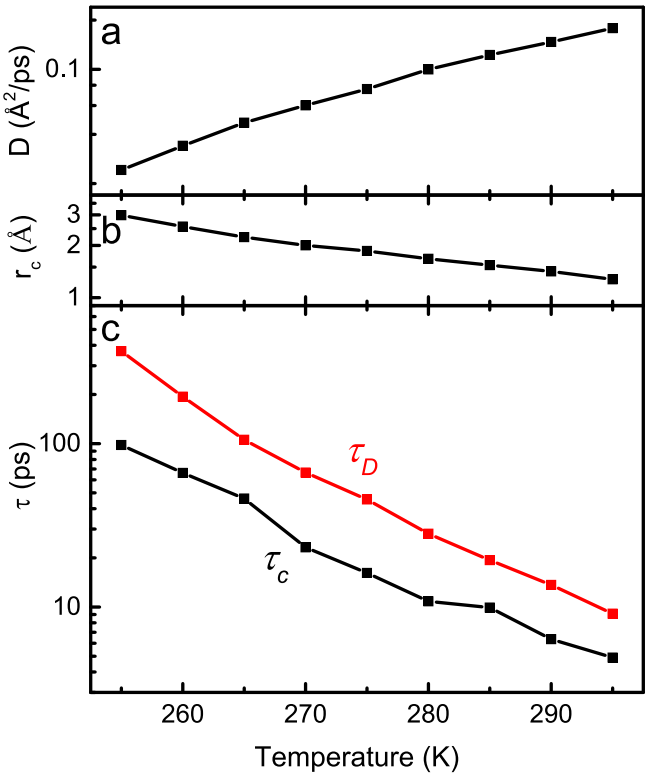

FIG. 6. Temperature dependence of ST2 water at density 0.95 g/cm^2 of (a) the self-diffusion constant D, (b) the correlation length r_c, and (c) the correlation time τ_c in black. Panel (c) also shows in red the diffusion time τ_D calculated according to Eq. (16).

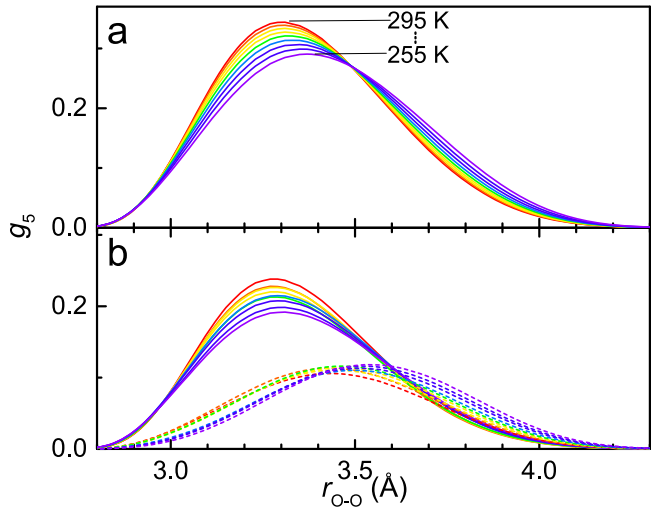

FIG. 7. (a) Radial distribution functions $g_5(r)$ of the 5th-closest water molecule around a central reference water molecule for TIP4P/2005 water with the temperature varied from T = 255 K (violet) to 295 K (red) in steps of 5 K at constant pressure of 1 bar. Panel (b) shows the same, but weighting each MD snapshot with the 2 localized probabilities $\boldsymbol{\rho}^{(1,loc)}$ and $\boldsymbol{\rho}^{(2,loc)}$.

whose length scales are much larger than what the order parameter measures. To see that this is indeed the case, we start with plotting spatial correlation functions in Fig. 5(b)

$$c_r(r) \equiv \frac{\langle p_i p_j \delta(r - r_{ij})\rangle}{\langle \delta(r - r_{ij})\rangle}, \tag{15}$$

where r_{ij} is the distance between the central waters i and j, p_i and p_j are the corresponding order parameters, respectively, and the average $\langle \ldots \rangle$ goes over time and all pairs of waters. The correlation function is normalized to the radial distribution function (the denominator in Eq. (15)) in order to reduce its oscillatory contribution. Again, the thin black lines in Fig. 5(b) represent exponential fits of the large-distance tails of $c_r(r)$,[52] with the resulting correlation lengths being summarized in Fig. 6(b).

With that, we can now see the connection between correlation time τ_c and correlation length r_c. It turns out that both are related by a simple expression

$$\tau_c \propto \tau_D \equiv \frac{r_c^2}{D}, \tag{16}$$

where τ_D is shown in red in Fig. 6(c). Here D is the self-diffusion constant of water (Fig. 6(a)), and the proportionality constant in Eq. (16) is a small numerical factor around 1/3. In simple words, the time τ_c (Fig. 6(c), black) it takes for a given water molecule to change its character between HDL and LDL-like is directly related to the time τ_D (Fig. 6(c), red) it needs to diffuse out of the corresponding domain with length-scale r_c (Fig. 6(b)). The correlation time has a much stronger temperature dependence than the correlation length, since the latter enters quadratically in Eq. (16) and since both the correlation length and diffusion constant contribute in a concerted way. Finally, the non-exponential decay of $c_t(t)$ originates from the fact that a water molecule at the border of a domain will interchange between domains much more quickly than a water molecule in the center of a domain.[53]

B. TIP4P/2005 water

After having established the method for ST2 water, we now turn to TIP4P/2005 water, which is the much more realistic representation of real water.[35,36] Qualitatively, the properties are still the same, and two-state behaviour can be identified in the temperature range from 255 K to 295 K. That is, the spectral analysis of the MSM still reveals one leading time-constant that is well separated from the all other time-constants (Fig. 2(b)). The time scale separation is smaller than that for ST2 water with $\tau_2/\tau_3 \approx 1.6$ at 255 K, but still sizeable.

Furthermore, despite the fact that the overall $g_5(r)$ shows no indication of a bimodal distribution at any temperature (Fig. 7(a)), the slowest time-constant τ_2 of the MSM still separates two subensembles, one HDL-like ensemble peaking at smaller distance r and one LDL-like ensemble peaking at larger distance r (Fig. 7(b)). Also the 3D distributions of these two subensembles, albeit being more smeared out, reveal very similar patterns as in the case of ST2 water (compare Fig. 4(b) with Fig. 4(a)).

The correlation times and correlation lengths are significantly smaller than for ST2 water (compare Fig. 8 with Fig. 5; note the different axes labelling) and also the variation with temperature is smaller, probably since the considered temperature range is further away from the hypothesized critical point. Other than that, the trends stay the same with the correlation time decreasing from 8.3 ps to 1.6 ps, and

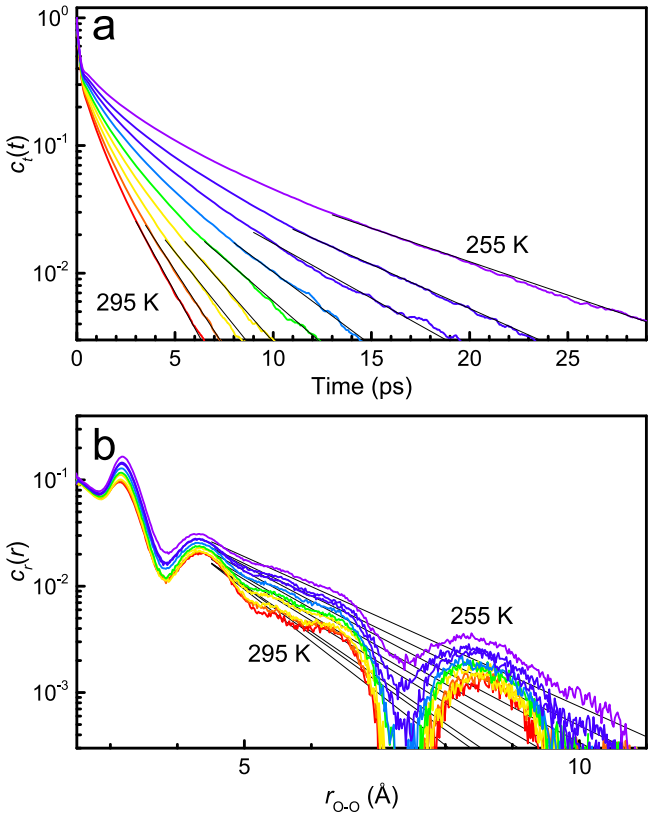

FIG. 8. (a) Time-correlation function $c_t(t)$ and (b) spatial correlation function $c_r(r)$ for TIP4P/2005 water at pressure 1 bar and the temperature varied from T = 255 K (violet) to 295 K (red). The thin black lines represent exponential fits to the long-time or large-distance tails of $c_t(t)$ and $c_r(r)$, respectively.

the correlation length decreasing from 1.5 Å to 1.1 Å, respectively, when increasing the temperature from 255 K to 295 K.

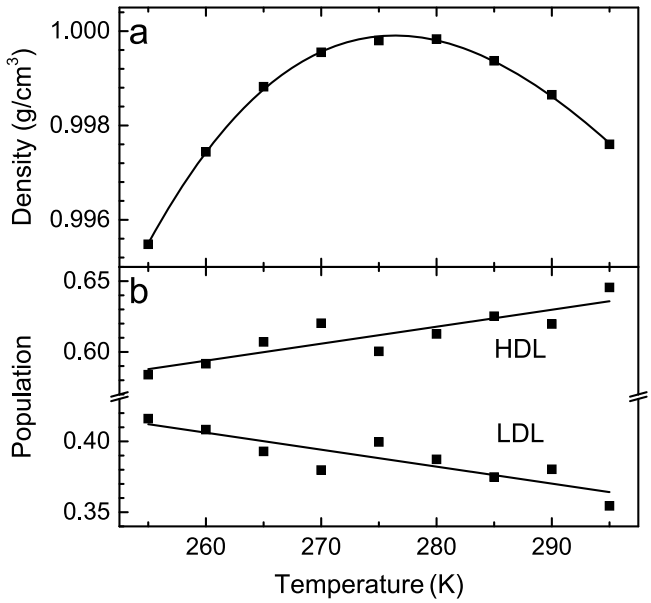

FIG. 9. (a) Density of TIP4P/2005 water as a function of temperature at 1 bar pressure together with a cubic fit and (b) statistical weight of the two sub-ensembles as a function of temperature (the solid lines represent linear fits to guide the eyes).

The most important result is the statistical weights of the two subensembles as a function of temperature (Fig. 9(b)). As one moves through the density maximum at 4 °C at constant pressure of 1 bar (which is correctly reproduced by the TIP4P/2005 water model, see Fig. 9(a)), the statistical weight of HDL-like water decreases with decreasing temperature. That is exactly how the two-state model of water attempts to explain the density maximum, i.e., the decreasing statistical weight of HDL-like water counteracts the otherwise expected monotonic increase in density with decreasing temperature.

IV. CONCLUSION

In conclusion, it has been shown that both ST2 and TIP4P/2005 water exhibit two-state behaviour for temperatures ranging from 255 K to room-temperature (295 K). In that temperature range, the slow and potentially diverging relaxation time, which hampers an unambiguous identification of a liquid-liquid critical point, is no longer an issue. Two-state behaviour is observed irrespective of the question whether that liquid-liquid critical point exists.

In order to identify two-state behaviour, an optimized order-parameter has been implemented. The only predetermined knowledge, which has been put into the construction of that order-parameter, is the fact that the 5th-closest water molecule is decisive. Hence, $(H_2O)_6$ clusters consisting of a central water molecule and the five closest water molecules around it have been considered. Other than that, no predetermined information has been included in the analysis, such as a geometry-based definition of a hydrogen bond[54] that we have used previously in a related study.[55] The structural similarity of two water clusters defined via their RMSD together with their kinetic connectivity along a MD trajectory have been used to coarse grain the ensemble of structures with the help of a MSM.

The resulting order parameter p_i (Eq. (13)) is defined by geometry only, i.e., for any arbitrary cluster structure one could determine whether it is HDL or LDL-like water, without having to know its past or future in the MD trajectory. It is a high-dimensional order parameter, in contrast to $g_5(r)$, and as such it has higher resolution power. For example, an interstitial water will to a certain extent also affect the positions of the neighboring waters in the first coordination layer. That is, the positions of all water molecules in the cluster are correlated, which is captured by the order parameter p_i, but not by $g_5(r)$. In contrast to the LSI,[21,22] on the other hand, the assignment to HDL or LDL water can be made directly from the local structure without having to quench the whole simulation box to 0 K. While the numerical costs of both approaches are comparable, that energy minimization step puts some question marks over the validity of the LSI as an order parameter.

In essence, the order parameter p_i is considered to be an improved version of $g_5(r)$, in the sense that the particular construct of the MSM started from the observation that $g_5(r)$ can discriminate HDL and LDL to a certain extent.[20] But

just like with "conventional" order parameters, two of which might highlight very different aspects of one and the same molecular systems, a differently constructed MSM might also give a different answer. There is no universal construct of a MSM.

Given that the MSM does detect a separation of time scales, albeit small in the case of TIP4P/2005 water, one must conclude that the distribution of structures is indeed bimodal and not continuous (which has been a matter of debate[18,19]). The time scale separation in the MSM goes along with multiple time scales in the time-correlation function $c_t(t)$, which reflects the fact that spatial domains of certain correlation lengths exist (Fig. 6). Hence, despite the fact that the MSM analyzes only the local structure around a given water, two-state behaviour is a collective phenomenon. One may assume that two-state behaviour deceases once the decay of $c_t(t)$ would become single-exponential.

TIP4P/2005 water is considered to be the best point-charge model of water.[36] That model of water can almost quantitatively describe recent SAXS data around room temperature, but an increasing temperature offset is needed for a semi-quantitative agreement with experiment in the supercooled regime.[56] In these experiments, the increasing scattering amplitude at small scattering angles is believed to result from exactly the spatial domains of HDL and LDL,[18] but their correlation length changes only minimally with temperature in TIP4P/2005 water (Fig. 8(b)). It will be very interesting to see how more involved, *ab-initio* based water models, such as MB-pol,[57] behave in this regard. Another possible extension of this work concerns the possibility that the so-called dynamical transition in proteins is correlated with a crossing of the Widom-line, i.e., that HDL or LDL water affects the dynamics of a protein differently.[58,59] Having developed a robust order parameter to discriminate HDL and LDL-like water, that effect should easily be detectable from all-atom MD simulations.

ACKNOWLEDGMENTS

I thank Andreas Vitalis for his help with the microstate clustering algorithm,[49] as well as Markus Meuwly, Amedeo Caflisch, Francesco Rao, and Frank Noé for valuable discussions. The work has been supported by the Swiss National Science Foundation (SNF) through the NCCR MUST.

[1]W. C. Röntgen, Ann. Phys. Chem. **281**, 91 (1892).
[2]P. G. Debenedetti, J. Phys.: Condens. Matter **15**, R1669 (2003).
[3]P. Poole, F. Sciortino, U. Essmann, and H. Stanley, Nature **360**, 324 (1992).
[4]O. Mishima and H. E. Stanley, Nature **396**, 329 (1998).
[5]J. A. Sellberg, C. Huang, T. A. McQueen, N. D. Loh, H. Laksmono, D. Schlesinger, R. G. Sierra, D. Nordlund, C. Y. Hampton, D. Starodub *et al.*, Nature **510**, 381 (2014).
[6]K. Amann-Winkel, C. Gainaru, P. H. Handle, M. Seidl, H. Nelson, R. Böhmer, and T. Loerting, Proc. Natl. Acad. Sci. U. S. A. **110**, 17720 (2014).
[7]Y. Liu, J. C. Palmer, A. Z. Panagiotopoulos, and P. G. Debenedetti, J. Chem. Phys. **137**, 214505 (2012).
[8]P. H. Poole, R. K. Bowles, I. Saika-Voivod, and F. Sciortino, J. Chem. Phys. **138**, 034505 (2013).
[9]J. C. Palmer, F. Martelli, Y. Liu, R. Car, A. Z. Panagiotopoulos, and P. G. Debenedetti, Nature **510**, 385 (2014).
[10]J. C. Palmer, F. Martelli, Y. Liu, R. Car, A. Z. Panagiotopoulos, and P. G. Debenedetti, Nature **513**, E2 (2016).
[11]D. Limmer and D. Chandler, J. Chem. Phys. **135**, 134503 (2011).
[12]D. Limmer and D. Chandler, J. Chem. Phys. **138**, 214504 (2013).
[13]D. Limmer and D. Chandler, Mol. Phys. **113**, 2799 (2015).
[14]D. Chandler, Nature **513**, E1 (2016).
[15]F. Smallenburg, L. Filion, and F. Sciortino, Nat. Phys. **10**, 653 (2014).
[16]F. Smallenburg and F. Sciortino, Phys. Rev. Lett. **115**, 015701 (2015).
[17]K. Binder, Proc. Natl. Acad. Sci. U. S. A. **111**, 9374 (2014).
[18]C. Huang, K. T. Wikfeldt, T. Tokushima, D. Norlund, Y. Harada, U. Bergmann, M. Niebuhr, T. M. Weiss, Y. Horikawas, M. Leetmaa *et al.*, Proc. Natl. Acad. Sci. U. S. A. **106**, 15214 (2009).
[19]G. N. I. Clark, G. L. Hura, J. Teixeira, A. K. Soper, and T. Head-Gordon, Proc. Natl. Acad. Sci. U. S. A. **107**, 14003 (2010).
[20]M. J. Cuthbertson and P. Poole, Phys. Rev. Lett. **106**, 115706 (2011).
[21]G. Appignanesi, J. A. R. Fris, and F. Sciortino, Eur. Phys. J. E **29**, 305 (2009).
[22]K. T. Wikfeldt, A. Nilsson, and L. G. M. Pettersson, Phys. Chem. Chem. Phys. **13**, 19918 (2011).
[23]G. Stirnemann and D. Laage, J. Chem. Phys. **137**, 031101 (2013).
[24]P. L. Geissler, C. Dellago, and D. Chandler, J. Phys. Chem. B **103**, 3706 (1999).
[25]G. R. Bowman, K. A. Beauchamp, G. Boxer, and V. S. Pande, J. Chem. Phys. **131**, 124101 (2009).
[26]J.-H. Prinz, H. Wu, M. Sarich, B. Keller, M. Senne, M. Held, J. D. Chodera, C. Schütte, and F. Noé, J. Chem. Phys. **134**, 174105 (2011).
[27]V. S. Pande, K. Beauchamp, and G. R. Bowman, Methods **52**, 99 (2010).
[28]J. D. Chodera and F. Noé, Curr. Opin. Struct. Biol. **25**, 135 (2014).
[29]F. H. Stillinger and A. Rahmann, J. Chem. Phys. **60**, 1545 (1974).
[30]P. H. Poole, I. Saika-Voivod, and F. Sciortino, J. Phys.: Condens Matter **17**, L431 (2005).
[31]Y. Liu, A. Z. Panagiotopoulos, and P. G. Debenedetti, J. Chem. Phys. **131**, 104508 (2009).
[32]P. H. Poole, S. B. Becker, F. Sciortino, and S. W. Starr, J. Phys. Chem. B **115**, 14176 (2011).
[33]T. A. Kesselring, E. Lascaris, G. Franzese, S. V. Buldyrev, H. J. Herrmann, and H. E. Stanley, J. Chem. Phys. **138**, 244506 (2013).
[34]T. A. Weber and F. H. Stillinger, J. Chem. Phys. **87**, 4277 (1983).
[35]J. L. F. Abascal and C. Vega, J. Chem. Phys. **123**, 234505 (2005).
[36]C. Vega and J. L. F. Abascal, Phys. Chem. Chem. Phys. **13**, 19663 (2011).
[37]J. L. F. Abascal and C. Vega, J. Chem. Phys. **133**, 234502 (2010).
[38]T. Sumi and H. Sekino, RSC Adv. **3**, 12743 (2013).
[39]J. Russo and H. Tanaka, Nat. Commun. **5**, 3556 (2014).
[40]R. S. Singh, J. W. Biddle, P. G. Debenedetti, and M. A. Anisimov, J. Chem. Phys. **144**, 144504 (2016).
[41]O. Steinhauser, Mol. Phys. **45**, 335 (1982).
[42]J. P. Ryckaert, G. Cicotti, and H. J. C. Berendsen, J. Comput. Phys. **23**, 327 (1977).
[43]D. van der Spoel, E. Lindahl, B. Hess, G. Groenhof, A. E. Mark, and H. J. C. Berendsen, J. Comput. Chem. **26**, 1701 (2005).
[44]W. Kabsch, Acta Crystallogr., Sect. A: Found. Adv. **A32**, 922 (1976).
[45]E. A. Coutsias, C. Seok, and K. A. Dill, J. Comput. Chem. **25**, 1849 (2004).
[46]A. Sadeghi, S. A. Ghasemi, B. Schaefer, S. Mohr, M. A. Lill, and S. Goedecker, J. Chem. Phys. **139**, 184118 (2013).
[47]Calculating the minimized RMSD of all 120 permutations does not yet require to calculate the transformation matrix from the SVD, only the corresponding singular values,[45] which is most efficiently done via the roots of the cubic characteristic polynomial (see http://www.rohitab.com/discuss/topic/36251-c-svd-of-3x3-matrix/). While this approach is potentially numerically unstable, it has been verified that the round-off errors are small for this particular problem. Only for the permutation that reveals the smallest RMSD, the full SVD is then calculated. See W. H. Press, S. A. Teukolsky, W. T. Vetterling, and B. P. Flannery, Numerical Recipes in C (Cambridge University Press, Cambridge, 1992).
[48]J. A. Hartigan, *Clustering Algorithms* (Wiley, New York, 1975), pp. 74–78.
[49]A. Vitalis and A. Caflisch, J. Chem. Theory Comput. **8**, 1108 (2012).
[50]C. Edmiston and K. Ruedenberg, Rev. Mod. Phys. **35**, 457 (1963).
[51]P. Hamm, J. Helbing, and J. Bredenbeck, Chem. Phys. **323**, 54 (2006).
[52]One expects $c_r(r)$ to go to zero for large enough r. However, due to the limited size of the simulation box and the fact that the MD simulation has been performed in the NVT ensemble, a small anti-correlation (i.e., negative $c_r(r)$) is observed for large r. Since LDL and HDL have different densities, a particular domain at one position of the simulation box implies a larger likelihood of the opposite domain far away from it since the total volume is constant. The fitting of the correlation function

therefore included a small negative pedestial, which has been subtracted in the presentation of Fig. 5(b).
[53]J. Borek, F. Perakis, and P. Hamm, Proc. Natl. Acad. Sci. U. S. A. **111**, 10462 (2014).
[54]R. Kumar, J. R. Schmidt, and J. L. Skinner, J. Chem. Phys. **126**, 204107 (2007).
[55]F. Rao, S. Garrett-Roe, and P. Hamm, J. Phys. Chem. B **114**, 15598 (2010).
[56]K. T. Wikfeldt, C. Huang, A. Nilsson, and L. G. M. Pettersson, J. Chem. Phys. **134**, 214506 (2011).
[57]G. R. Medders, V. Babin, and F. Paesani, J. Chem. Theory Comput. **10**, 2906 (2014).
[58]S.-H. Chen, L. Liu, E. Fratini, P. Baglioni, A. Faraone, and E. Mamontov, Proc. Natl. Acad. Sci. U. S. A. **103**, 9012 (2006).
[59]P. Kumar, Z. Yan, L. Xu, M. G. Mazza, S. Buldyrev, S.-H. Chen, S. Sastry, and H. E. Stanley, Phys. Rev. Lett. **97**, 177802 (2006).